Ceramics International, Volume 45, Issue 9, June 2019, pp. 11749-11755
DOI:10.1016/j.ceramint.2019.03.051

High-performance La-doped BCZT thin film capacitors on $LaNiO_3$/Pt composite bottom electrodes with ultra-high efficiency and high thermal stability

Shangkai He[1,2], Biaolin Peng[1,2]*, Glenn J.T. Leighton[2], Christopher Shaw[2], Wenhong Sun[1], Ningzhang Wang[1**], Qi Zhang[2***]

[1]Center on Nanoenergy Research, School of Physical Science & Technology, Guangxi University, Nanning 530004, China

[2]Department of Manufacturing and Materials, Cranfield University, Cranfield, Bedfordshire, MK43 0AL, United Kingdom

*Correspondence to: pengbl8@126.com, 20180001@gxu.edu.cn, Q.zhang@cranfield.ac.uk

Abstract:

Dielectric capacitors possessing large energy storage density, high efficiency and high thermal stability simultaneously are very attractive in modern electronic devices to be operated in harsh environment. Here, it is demonstrated that large energy storage density (W ~ 15.5 J/cm^3) simultaneously with ultra-high efficiency (η ~ 93.7%) and high thermal stability (the variation of both W from 20 °C to 260 °C and η from 20°C to 140 °C is less than 5%) have been achieved in the La-doped $(Ba_{0.904}Ca_{0.096})_{0.9775+x}La_{0.015}(Zr_{0.136}Ti_{0.864})O_3$ (x = 0.0075) lead-free relaxor ferroelectric thin film capacitors deposited on $LaNiO_3$/Pt composite bottom electrodes by using a sol-gel method. The great energy storage property of the thin film capacitors at x = 0.0075 is mainly ascribed to the diversity of the structure of the nano-clusters around the three-phases coexisting component point $(Ba_{0.904}Ca_{0.096})(Zr_{0.136}Ti_{0.864})O_3$ where cubic, tetragonal and rhombohedral phases coexisted, as well as the ultra-high quality of thin film due to the utilization of the $LaNiO_3$/Pt composite bottom electrode, making it a promising candidate for dielectric capacitors working in harsh environments.

Keywords: dielectric capacitors; sol-gel; thin film; energy storage.

1. Introduction

Recently, there is increasing attention paid to dielectric capacitors due to their excellent storage characteristics, such as high power density, fast charge/discharge capability, low cost, lifetime and excellent mechanical stability, etc.[1-3]. Especially, the power density of dielectric capacitors is 2-5 orders of magnitude larger than those of electrochemical energy storage devices such as batteries. These outstanding advantages make them ideal candidates for application in high-power electrical energy storage systems, such as power electronics and pulsed power equipment in electric vehicles, solar or wind power generation systems, etc. However, the much lower energy density compared with electrochemical energy storage devices still restrict their wider application. Thus, to dramatically enhance the energy density in dielectric capacitors is a considerable interesting thing to do.

For dielectric capacitors, the energy storage properties are characterized by the polarization-electric field (*P*-*E*) loops and the recoverable energy density (W_{rec}) and the efficiency (η) are estimated with the following equations:

$$W = \int_{P_r}^{P_{max}} E\, dP \tag{1}$$

$$\eta = \frac{W}{W + W_{loss}} \tag{2}$$

where P_{max} and P_r are the maximum polarization and the remnant polarization, respectively. E is the applied field, and P means polarization. W_{loss} represents the lost energy density. Obviously, possessing large P_m, small P_r, high E and low W_{loss} simultaneously is essential to achieve large W_{rec} and high η in dielectric capacitors. Apart from large W_{rec} and high η, the thermal stability is also another vital property for dielectric capacitors, especially for those working in harsh environments. For instance, electronic equipment working in the temperature range of 150 °C to 200 °C without a cooling system should possess the ability to overcome the high temperature harsh conditions.

With the rapid development of modern thin film preparation technology (sol-gel, pulsed laser deposition (PLD), and molecular beam epitaxy, etc.), many high-performance lead-based antiferroelectric (AFE) thin films materials with large W_{rec} has been obtained due to the significantly improved dielectric breakdown strength (> 1000 kV/cm), such as 56 J/cm^3 at 3500 kV/cm in

$(Pb_{0.97}La_{0.02})(Zr_{0.55}Sn_{0.4}Ti_{0.05})O_3$ AFE thin film (1.8 μm in thickness), 40.18 J/cm^3 at 2801 kV/cm in $Pb_{0.8}Ba_{0.2}ZrO_3$ AFE/FE coexisted thin film (320 nm in thickness), 18.8 J/cm^3 at 900 kV/cm in 3 mol% Eu-doped $PbZrO_3$ AFE thin film and 11.7 J/cm^3 at 1200 kV/cm in $Pb_{0.97}La_{0.02}(Zr_{0.97}Ti_{0.03})O_3$ AFE thin film (400 nm in thickness). These breakthroughs in lead-based AFE thin film materials will promote modern high-power electrical energy storage systems move toward high integration, miniaturization and light weight for portability. Nevertheless, the poor η (usually less than 60%) in AFE materials, as well as the great toxicity of lead to the environment and human beings, severely limits their applications as energy storage devices. To look for lead-free AFE materials that are comparable to lead-based AFE materials, many research works have been done. One of the most outstanding representatives is that a very high W_{rec} of ~ 61.2 J/cm^3 with a η of ~ 65% at 4500 kV/cm has been obtained in Si-doped (6.0 mol. %) HfO_2 AFE thin films (10 nm in thickness) prepared by an ALD method. In addition, a W of 21.3 J/cm^3 with a η of 75% at 4250 kV/cm in the linear dielectric HfO_2 thin film (63 nm in thickness) and a W of 46 J/cm^3 with a η of ~ 51% at 4500 kV/cm in $Hf_{0.3}Zr_{0.7}O_3$ AFE thin film (9.2 nm in thickness) were also obtained. However, the W value decreased significantly with increasing film thickness in these HfO_2-based thin films, such as the W value of $Hf_{0.3}Zr_{0.7}O_3$ AFE thin films dropped sharply from 46 J/cm^3 to 21 J/cm^3 as the thickness of thin films increased from 9.2 nm to 19.0 nm, indicating that the development of their application in dielectric energy storage systems could be restricted severely. Although a high W value of 78.7 J/cm^3 at 6600 kV/cm and an ultrahigh W value of 154 J/cm^3 at 3500 kV/cm have also been obtained for the $BaZr_{0.35}Ti_{0.65}O_3$ relaxor thin film (440 nm in thickness) prepared by a radio-frequency sputtering technology and the BNLBTZ AFE/FE coexisted epitaxial thin film (350 nm in thickness) prepared by a PLD method, respectively, the expensive cost of single substrates (Nb-doped $SrTiO_3$ and $SrTiO_3$) seems limit their practical applications. In addition, the W value could exceed 10 J/cm^3 has also been obtained in some poly (vinylidenefluoride) PVDF or their inorganic FE composites (FE/PVDF). However, their operating temperatures were very strictly limited to a low temperature (usually lower than 85 °C) due to the bad thermal stability, indicating that they are suitable for working in high-temperature harsh environments.

In this work, the three-phases (cubic, tetragonal and rhombohedral phases) coexisting component point 0.68BZT-0.32BCT (pure BCZT) is chosen to be the basic component of the $(Ba_{0.904}Ca_{0.096})_{0.9775+x}La_{0.015}(Zr_{0.136}Ti_{0.864})O_3$ (abbreviated as La-doped BCZT, and x = 0.0075, 0.075

and 0.15) dielectric relaxor thin film capacitors prepared by using a sol-gel method (low cost, high preparation efficiency, good repeatability and large-scale industrialization, etc.). A dopant of La^{3+} element accompanied by excess $(Ba_{0.904}Ca_{0.096})^{2+}$ is employed to create non-stoichiomechic A-site ions in the perovskite structure, which were considered as an effective strategy to modify the relaxor behavior of dielectrics. Large energy storage density (W ~ 15.5 J/cm^3) simultaneously with ultra-high efficiency (η ~ 93.7%) and high thermal stability (the variation of both W from 20 °C to 260 °C and η from 20°C to 140 °C is less than 5%) were achieved at x = 0.0075, which were much better than those of polymer-, lead-based AFE and HfO_2-based AFE materials, etc. The diversity of the structure of the nano-clusters around the three-phases coexisting component point and the ultra-high quality of thin film due to the utilization of the $LaNiO_3$/Pt composite bottom electrode co-play an important role in achieving the great energy storage property, especially in its thermal stability. These findings provide a guide for synthesizing high-performance thin film capacitors working in harsh environments.

2. Experimental process

Pure and La-doped BCZT thin films were prepared by using a sol-gel method, as shown in **Fig. S2a**. Barium acetate ($Ba(CH_3COOH)_2$) and calcium acetate ($Ca(CH_3COOH)_2$) were dissolved in 120 □ glacial acetic acid. Meanwhile, zirconium isopropoxide ($Zr(OC_3H_7)_4$) and tetrabutyl titanate ($Ti(OC_4H_9)_4$) were dissolved in a mixture of glacial acetic and acetylacetone at room temperature. For the La-doped BCZT thin film, lanthanum acetate hydrate ($C_6H_9O_6La{\cdot}xH_2O$) was also introduced into the Ba/Ca solution. Then the two solutions were mixed and stirred for 30 min at 100 □. Subsequently, the concentration of the final solution was adjusted to 0.2 M by adding appropriate additives. When aged for 24 h, the precursor solutions were deposited on Pt(111)/TiOx/SiO_2/Si (abbreviated as Pt) and $LaNiO_3$/ Pt(111)/TiOx/SiO_2/Si (abbreviated as $LaNiO_3$/Pt) substrates, which were rinsed with acetone and ethanol, respectively. After each spin-coating process, the wet film was firstly dried at 200 □ for 5 min, then pyrolyzed at 415 □ for 5 min on a hotplate, and finally it was placed into a crucible and was annealed at 700 □ for 3 min in a tube furnace. The above process was repeated for 8 times to obtain the final thin films.

The layer of $LaNiO_3$ was prepared by the previous method, as shown in **Fig. S2b.** Lanthanum nitrate

($La(NO_3)_3$) and nickel acetate ($Ni(CH_3COOH)_2$) were dissolved in a mixture of glacial acetic acid, water and formamide (CH_3NO) at room temperature. The final concentration of the $LaNiO_3$ precursor solution was 0.3 M. When aged for 24 h, the solution was deposited on a Pt(111)/TiOx/SiO_2/Si substrate by spin-coating at 4000 rpm for 40 s. Each wet layer was firstly dried at 180 □ for 5 min, then pyrolyzed at 450 □ for 5 min on a hotplate, and finally it was annealed at 700 □ for 5 min in a tube furnace. The above process was repeated for 6 times.

The crystalline structures of the pure and La-doped BCZT thin films were measured by the X-ray diffraction (XRD; Rigaku 9 KW Smartlab, Tokyo, Japan). The surface morphology and cross-sectional micrographs of the thin films were observed by the field emission scanning electron microscopy (FE-SEM; Hitachi SU8220, Japan). To measure the electrical properties, Cr/Au top electrodes with a square pattern and a size of 90 μm × 90 μm were deposited by the plasma sputtering with a shadow mask. Dielectric properties were measured by using an impedance analyzer (Agilent E4980A, USA) under a perturbation voltage of 0.5 V. The hysteresis loops between polarizations and electric fields (*P-E* loops) were evaluated by using a ferroelectric tester (Radiant Precision Premier □, USA).

3. Results and discussion

3.1 Structure

Fig. 1 shows the XRD patterns of pure and La-doped BCZT thin films deposited on Pt bottom electrodes and $LaNiO_3$/Pt composite bottom electrodes. No matter whether the thin films were deposited on the Pt bottom electrodes or on the $LaNiO_3$/Pt composite bottom electrodes, all thin films exhibit pure perovskite structures with a strong (111) orientation and without any secondary phase. In addition to the (111) peak, a weak (002) peak can also be observed. Compared to the pure BCZT thin film deposited on the Pt bottom electrode, an additional weak (200) peak can also be detected for the pure BCZT thin film deposited on the $LaNiO_3$/Pt composite bottom electrode, indicating that the appearance of the tetragonal phase could be ascribed to the thermal stress due to the difference of thermal expansion coefficients between the BCZT and the $LaNiO_3$ oxide layers. However, the (200) peak disappeared when the La element was doped, resulting in a stronger (002) peak. The above results reveal that the phase structure of the pure BCZT thin films including not

only the one directly deposited on the Pt bottom electrode and but also the one deposited on the $LaNiO_3$/Pt composite bottom electrode could be deviated from the designed triple-point where the Cubic phase, the tetragonal phase and the rhombohedral phase coexisted. Moreover, with the increase of the excess $(Ba_{0.904}Ca_{0.096})^{2+}$, the (111) peak of the thin films deposited on the $LaNiO_3$/Pt composite bottom electrodes shift toward the lower angle, indicating that the lattice parameter around the triple-point phase is also sensitive to the excess $(Ba_{0.904}Ca_{0.096})^{2+}$.

As a representative, **Fig. 2** shows the cross-sectional SEM images of the La-doped BCZT thin films at x = 0.075 deposited on the Pt bottom electrodes and the La-doped BCZT thin films at x = 0.15 deposited on the $LaNiO_3$/Pt composite bottom electrodes. The thickness of both samples is about 280 nm, indicating that the effect of both composition and substrate is negligible to the thickness of thin films under the same preparation parameters. All Pt bottom electrodes exhibit a columnar structure, which favors the formation of the (111) orientation. The interfaces between the Pt bottom electrodes and the thin films including the BCZT layer and the $LaNiO_3$ oxide layer are all clear and visible. However, for the samples deposited on the $LaNiO_3$/Pt composite bottom electrodes, the interfaces between the BCZT thin films and the $LaNiO_3$ oxide layers are hard to distinguish, indicating a good lattice match, as shown by the overlapping XRD diffraction peaks.

3.2 Dielectric properties

Fig. 3 shows the temperature dependence of the dielectric permittivity (ε) and the dielectric loss ($tan\ \delta$) of pure and La-doped BCZT thin films. Compared to the thin films deposited on Pt bottom electrodes, the corresponding films deposited on $LaNiO_3$/Pt composite bottom electrodes exhibit a larger ε value and a smaller $tan\ \delta$ value at the whole measuring temperature range. Generally, the dielectric permittivity of thin films could be affected by several factors, such as the orientation, defects and stress, etc. The orientations of thin films are all (111) orientations, indicating that the orientations have a week impact on the ε value. Some B-site defects such as oxygen vacancies favor to couple with A-site vacancies to form defect dipoles. The dielectrics possessing a high concentration of defect dipoles often tend to exhibit a larger ε value and also a high dielectric loss value, especially at the low frequencies. The contribution of the defect dipoles to the larger ε value and smaller tan δ value of the thin films deposited on $LaNiO_3$/Pt composite bottom electrodes can be excluded, since their ε values are smaller than those of thin film deposited on Pt bottom electrodes at

the low frequencies, as shown in the **Fig. S3**. One possible reason is that the phase structures of thin films change when the $LaNiO_3$ oxide layers are used, and the phase transition temperature was promoted to a higher temperature. As a result, a larger ε value and a smaller *tan* δ value are obtained in the thin films deposited on $LaNiO_3$/Pt composite bottom electrodes rather than that directly deposited on Pt bottom electrodes. Among all thin films, the highest value of dielectric permittivity at room temperature is obtained in the pure BCZT thin film deposited on $LaNiO_3$/Pt composite bottom electrode, which is attributed to the existence of tetragonal phase, as shown in the XRD patterns. With the doping of the La element and the increase of the excess $(Ba_{0.904}Ca_{0.096})^{2+}$, the value of ε tends to decrease, as shown in the **Fig. 3 b)**, **d)**, **f)** and **h)**.

3.3 Energy storage

Fig. 4 shows the *P-E* loops of pure and La-doped BCZT thin films at selected electric fields at 10 kHz at room temperature. All thin films deposited on the $LaNiO_3$/Pt composite bottom electrodes exhibit a higher polarization and lower hysteresis loss (slimmer *P-E* loops) than those directly deposited on the Pt bottom electrodes, especially for the pure BCZT thin film and the La-doped thin film at x = 0.15. Previous research works indicate that this phenomenon could be ascribed to the reduced concentrations of oxygen vacancies and space charges in thin films, which are the main source of ferroelectric domains pinning center and high leakage current. Another possible factor is that the decreased lattice mismatch between the BCZT thin films and $LaNiO_3$ improves crystalline quality and reduces mechanical stress in the films. The recoverable energy density (W) and energy storage efficiency (η) at selected electric fields are shown in the insets of **Fig. 4**. The W values tend to increase with the increase of applied electric field for all thin films. The η values of the thin films deposited on the Pt bottom electrodes tend to deteriorate with the increase of applied electric field, especially for the pure BCZT thin films and La-doped at x = 0.15. For example, the η values of the thin film at x = 0.15 has been dropped from 92.4% at 703 kV/cm to 64.4% at 3335 kV/cm. However, the η values of the thin films deposited on $LaNiO_3$/Pt composite bottom electrodes tend to keep them at a constant level, and the η values of the pure, x = 0.0075, x = 0.075 and x = 0.75 are 84.7%, 93.7%, 91.5% and 87.4% at 3335 kV/cm, respectively. The largest W (15.5 J/cm^3) is obtained in the La-doped thin film deposited on the $LaNiO_3$/Pt composite bottom electrode at x = 0.0075. With the further increase of the amount of the excess $(Ba_{0.904}Ca_{0.096})^{2+}$, the W value tends to decrease,

indicating a degraded performance of energy storage. It should be noted that the *W* value could be further enhanced when the applied electric field increases.

In addition to large *W* value and high η value, a good thermal stability is also expected in practical applications of capacitors. **Fig. 5** shows the temperature dependences of the *W* and η obtained from the *P-E* loops (see **Fig. S4**) of thin films deposited on $LaNiO_3$/Pt composite bottom electrodes. Compare to the pure BCZT thin film, the *W* value of the thin film at x = 0.0075 almost keeps constant in the whole temperature range, and the variation of *W* from 20 °C to 260 °C is less than 5%, as shown by the red solid line. It is much better than those of polymer-, lead-based AFE and HfO_2-based AFE materials, etc., indicating that the thin film is a promising candidate for dielectric capacitors working in harsh environments. As the amount of the excess $(Ba_{0.904}Ca_{0.096})^{2+}$ is further increased, the thermal stability tends to degrade slightly, as shown by the blue and dark cyan down-arrows. Compared with the thermal stability of the *W*, the thermal stability of the η tends to weaken, as shown by the up-arrows. For example, the η value of the thin film at x = 0.0075 is as high as 92.3% in the temperature range of 20 □ to 140 °C (the variation of η is less than 5%), but it sharply dropped to 75.7% as the temperature increased to 260 □, which may be caused by the increasing leakage current as the operating temperature increases. It should be noted that the good thermal stability is related not only to the great dielectric relaxor diffusion dominated by the diversity of the structure of the nano-clusters around the three-phases coexisting component point $(Ba_{0.904}Ca_{0.096})(Zr_{0.136}Ti_{0.864})O_3$ where cubic, tetragonal and rhombohedral phases coexisted, as shown by the phase diagram in Fig.S1, but also to the ultra-high quality of thin film due to the utilization of the $LaNiO_3$/Pt composite bottom electrode, since that both *W* and η of the thin film at x = 0.0075 deposited on the Pt bottom electrode drop sharply as the operating temperature increases, as shown in the inset of **Fig. 5**.

It is well known that the dielectric breakdown strength of thin film capacitors becomes lower with the increase of the electrode area because the number of defects is possibly increasing such as gas holes and micro-cracks, etc. Therefore, thin films capacitors possessing a large operational electrode area as much as possible is expected in practical applications. However, to our knowledge, few research works relating to this case have been reported. To get an insight into the problem, the thin films at x = 0.0075 coated with four different sizes of Pt top electrodes rather than Au/Cr top electrodes were investigated. According to the sizes (see **Table S1**) of the Pt top electrodes, the thin

film samples were classified as S_1, S_2, S_3 and S_4, respectively. **Fig. 6** shows the top electrode area dependence of energy storage properties. Obviously, the W value drops sharply from 9.5 J/cm^3 to the 2.7 J/cm^3 as the top electrode area increases from the ~ 0.025 mm^2 of S_1 to the ~ 0.785 mm^2 of S_2, since the operational electric field decreases sharply (see **Fig. S5**). However, the η value can always keep at a very high level with the increase of top electrode area. For example, although the W value of the thin film deposited on $LaNiO_3$/Pt composite electrode is only 0.7 J/cm^3, the η value is still as high as 91.4% when the area of top electrode has been increased to ~ 7.709 mm^2. It should be noted that the dropping operational electric field could not be ascribed to the dielectric breakdown of the thin film. One possible factor is that the Pt top electrode is ablated partly, as shown by the black arrow in the inset of the **Fig. 6**. By contrast, the thin film is still intact, as shown by the red arrow in the inset of the **Fig. 6**. Furthermore, the dielectric breakdown field of the top electrode with larger size could be optimized by the use of some oxide electrodes such as $LaNiO_3$ and ITO, etc. The implantation of the "dead layers" (Al_2O_3 and HfO_2, etc.) between top electrode and thin film is also another feasible method.

4. Conclusion

La-doped $(Ba_{0.904}Ca_{0.096})_{0.9775+x}La_{0.015}(Zr_{0.136}Ti_{0.864})O_3$ lead-free relaxor ferroelectric thin films deposited on $LaNiO_3$/Pt composite bottom electrodes were prepared by using a sol-gel method. For the thin films capacitors, large energy storage density (W ~ 15.5 J/cm^3), ultra-high efficiency (η ~ 93.7%) and high thermal stability (the variation of both W from 20 °C to 260 °C and η from 20°C to 140 °C are less than 5%) are simultaneously obtained at x = 0.0075. Both the diversity of the structure of the nano-clusters around the three-phases coexisting component point and the ultra-high thin film quality because of the utilization of the $LaNiO_3$/Pt composite bottom electrode are responsible for the high energy storage performance. Moreover, a larger size of top electrode operated under a higher dielectric breakdown field could be further optimized. These excellent results indicate that the La-doped thin film capacitors are promising candidates for dielectric capacitors working in harsh environments.

Acknowledgments

This work was supported by the National Natural Science Foundation of China (51402196、51602159), the Guangxi Natural Science Foundation (Grants 2016GXNSFCB380006, 2017GXNSFFA198015), and the Scientific Research Foundation of Guangxi University (Grant XTZ160530), Bagui Rencai & Bagui Xuezhe Funding (Grant C31200992001).

Reference

[1] Z. Pan, L. Yao, J. Zhai, X. Yao, H. Chen, Interfacial Coupling Effect in Organic/Inorganic Nanocomposites with High Energy Density, Advanced materials, 30 (2018) e1705662.

[2] X. Zhang, Y. Shen, B. Xu, Q. Zhang, L. Gu, J. Jiang, J. Ma, Y. Lin, C.W. Nan, Giant Energy Density and Improved Discharge Efficiency of Solution-Processed Polymer Nanocomposites for Dielectric Energy Storage, Advanced materials, 28 (2016) 2055-2061.

[3] K. Han, Q. Li, C. Chanthad, M.R. Gadinski, G. Zhang, Q. Wang, A Hybrid Material Approach Toward Solution-Processable Dielectrics Exhibiting Enhanced Breakdown Strength and High Energy Density, Advanced Functional Materials, 25 (2015) 3505-3513.

[4] S.A. Sherrill, P. Banerjee, G.W. Rubloff, S.B. Lee, High to ultra-high power electrical energy storage, Physical chemistry chemical physics : PCCP, 13 (2011) 20714-20723.

[5] N.S. Choi, Z. Chen, S.A. Freunberger, X. Ji, Y.K. Sun, K. Amine, G. Yushin, L.F. Nazar, J. Cho, P.G. Bruce, Challenges facing lithium batteries and electrical double-layer capacitors, Angewandte Chemie, 51 (2012) 9994-10024.

[6] P. Khanchaitit, K. Han, M.R. Gadinski, Q. Li, Q. Wang, Ferroelectric polymer networks with high energy density and improved discharged efficiency for dielectric energy storage, Nature communications, 4 (2013) 2845.

Figures and Captions

Figure 1. XRD patterns of pure and La-doped BCZT thin films. a) On Pt bottom electrodes, b) on $LaNiO_3$/Pt composite bottom electrodes.

Figure 2. Cross-sectional SEM images of La-doped BCZT thin films at x = 0.0075. a) On Pt bottom electrodes, b) on $LaNiO_3$/Pt composite bottom electrodes.

Figure 3. Temperature dependence of dielectric permittivity and dielectric loss of pure and La-doped BCZT thin films. a), c), e) and g) on Pt bottom electrodes; b), d), f) and h) on $LaNiO_3$/Pt composite bottom electrodes.

Figure 4. *P*-*E* loops of pure BCZT and La-doped BCZT thin films at selected fields. a), c), e) and g) on Pt bottom electrodes; b), d), f) and h) on $LaNiO_3$/Pt composite bottom electrodes. Insets in the right lower corners of a) - h): W and η.

Figure 5. $W(T)$ and $\eta(T)$ of pure and La-doped BCZT thin films on $LaNiO_3$/Pt composite bottom electrodes.

Figure 6. The area of top electrode as a function of W and η of La-doped BCZT thin films at x = 0.0075 on $LaNiO_3$/Pt composite bottom electrodes. Inset: image of Pt top electrode.

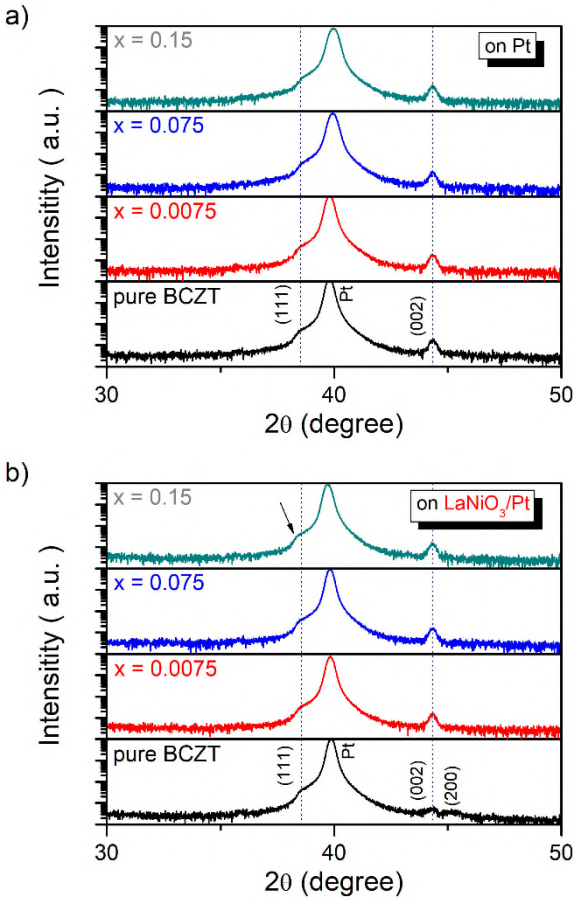
a)
x = 0.15
on Pt
x = 0.075
x = 0.0075
pure BCZT
(111)
Pt
(002)
Intensitity (a.u.)
30
40
50
2θ (degree)
b)
x = 0.15
on LaNiO3/Pt
x = 0.075
x = 0.0075
pure BCZT
(111)
Pt
(002)
(200)
Intensitity (a.u.)
30
40
50
2θ (degree)

Figure 1

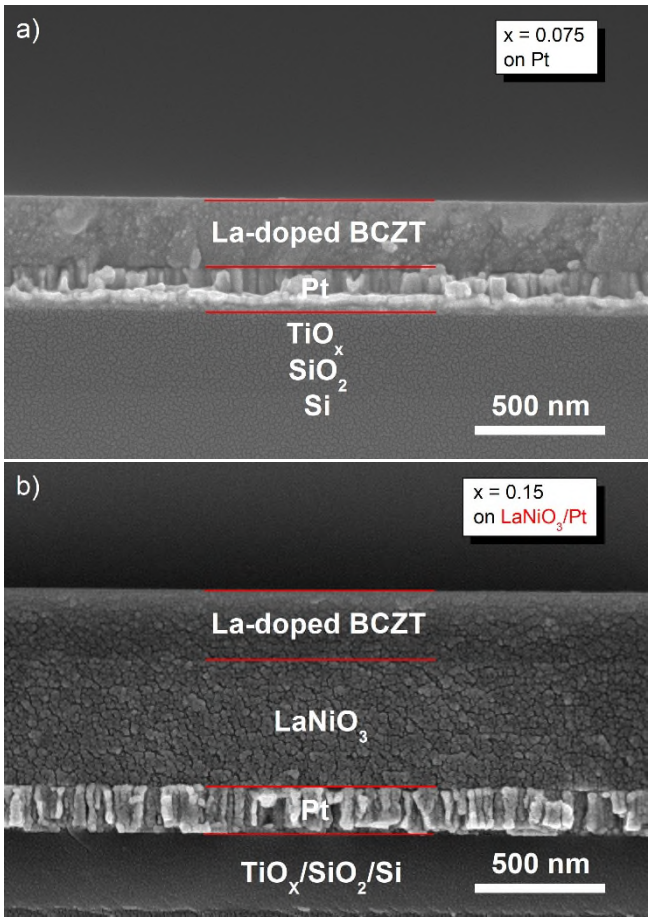
a)
x = 0.075
on Pt
La-doped BCZT
Pt
TiOx
SiO2
Si
500 nm
b)
x = 0.15
on LaNiO3/Pt
La-doped BCZT
LaNiO3
Pt
TiOx/SiO2/Si
500 nm

Figure 2

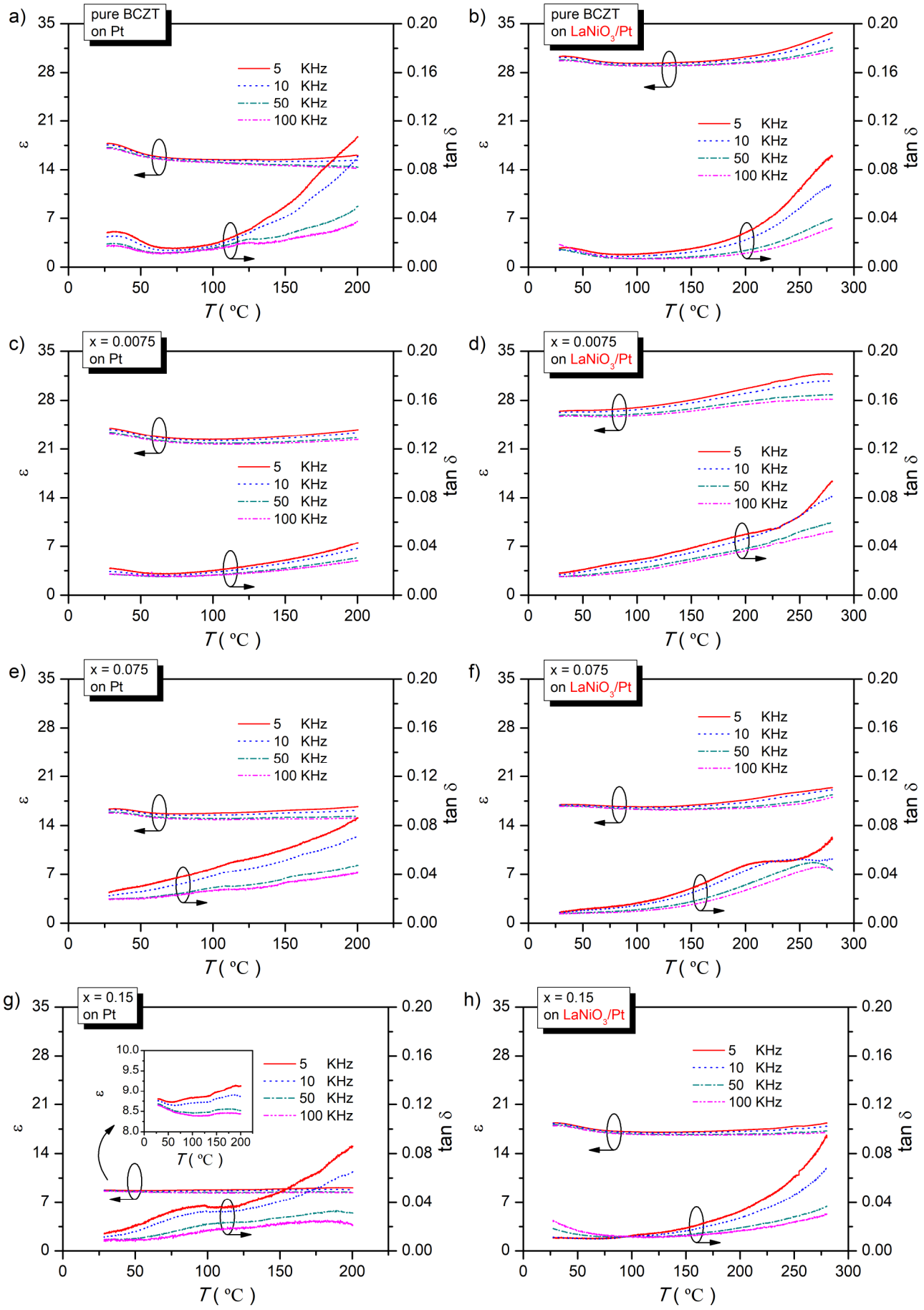
a)
pure BCZT
on Pt
b)
pure BCZT
on LaNiO3/Pt
c)
x = 0.0075
on Pt
d)
x = 0.0075
on LaNiO3/Pt
e)
x = 0.075
on Pt
f)
x = 0.075
on LaNiO3/Pt
g)
x = 0.15
on Pt
h)
x = 0.15
on LaNiO3/Pt
5 KHz
10 KHz
50 KHz
100 KHz
ε
tan δ
T (℃)

Figure 3

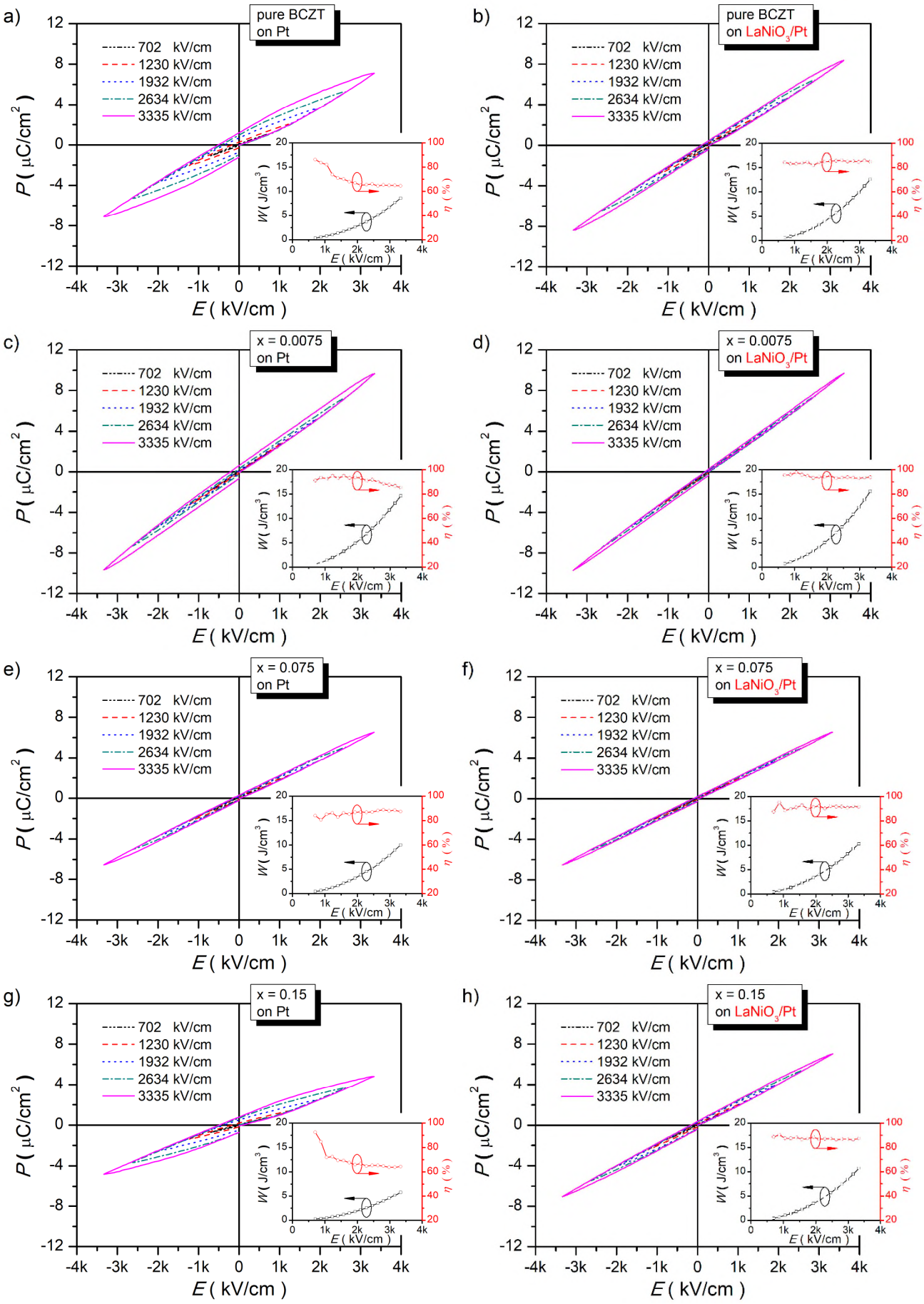
a)
pure BCZT on Pt
b)
pure BCZT on LaNiO3/Pt
c)
x = 0.0075 on Pt
d)
x = 0.0075 on LaNiO3/Pt
e)
x = 0.075 on Pt
f)
x = 0.075 on LaNiO3/Pt
g)
x = 0.15 on Pt
h)
x = 0.15 on LaNiO3/Pt
702 kV/cm
1230 kV/cm
1932 kV/cm
2634 kV/cm
3335 kV/cm
P (μC/cm2)
E (kV/cm)
W (J/cm3)
η (%)

Figure 4

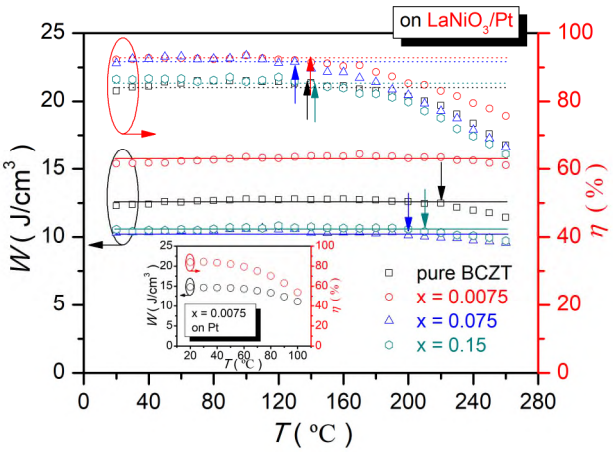
on LaNiO3/Pt
W (J/cm3)
η (%)
T (℃)
pure BCZT
x = 0.0075
x = 0.075
x = 0.15
x = 0.0075
on Pt

Figure 5

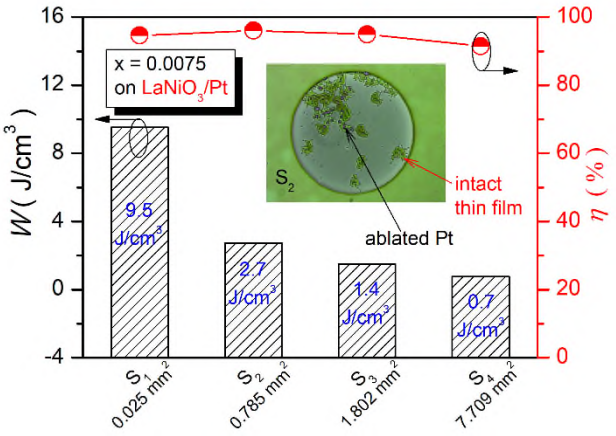
x = 0.0075
on LaNiO3/Pt
W (J/cm3)
η (%)
9.5 J/cm3
2.7 J/cm3
1.4 J/cm3
0.7 J/cm3
S2
intact thin film
ablated Pt
S1 0.025 mm2
S2 0.785 mm2
S3 1.802 mm2
S4 7.709 mm2

Figure 6

Supplementary materials for

High-performance La-doped BCZT thin film capacitors on $LaNiO_3$/Pt composite bottom electrodes with ultra-high efficiency and high thermal stability

Shangkai He[1,2], Biaolin Peng[1,2]*, Glenn J.T. Leighton[1], Christopher Shaw[1], Wenhong Sun[2], Ningzhang Wang[2], Qi Zhang[1]*

[1]Department of Manufacturing and Materials, Cranfield University, Cranfield, Bedfordshire, MK43 0AL, United Kingdom

[2]Center on Nanoenergy Research, School of Physical Science & Technology, Guangxi University, Nanning 530004, China

*Correspondence to: pengbl8@126.com, Q.zhang@cranfield.ac.uk

This PDF file includes:

Figure S1 to S5, and Table S1

Figure S1. Phase diagram of pseudobinary ferroelectric system $Ba(Zr_{0.2}Ti_{0.8})O_3$-$(Ba_{0.7}Ca_{0.3})TiO_3$.

Figure S2. Flow charts of a) pure and La-doped BCZT thin films and b) $LaNiO_3$ bottom electrodes prepared by sol-gel methods.

Figure S3. Frequency dependence of dielectric permittivity and dielectric loss of pure and La-doped BCZT thin films. a) On Pt bottom electrodes, b) on $LaNiO_3$/Pt composite bottom electrodes.

Figure S4. *P*-*E* loops of pure BCZT and La-doped BCZT thin films on $LaNiO_3$/Pt composite bottom electrodes at selected temperatures. a) pure BCZT, b) x = 0.0075, c) x= 0.075 and d) x = 0.15.

Figure S5. *P*-*E* loops with various sizes of Pt top electrodes of La-doped BCZT thin films at x = 0.0075 on $LaNiO_3$/Pt composite bottoms.

Table S1. Energy storage performance of La-doped BCZT thin films at x = 0.0075 on $LaNiO_3$/Pt composite bottom electrodes.

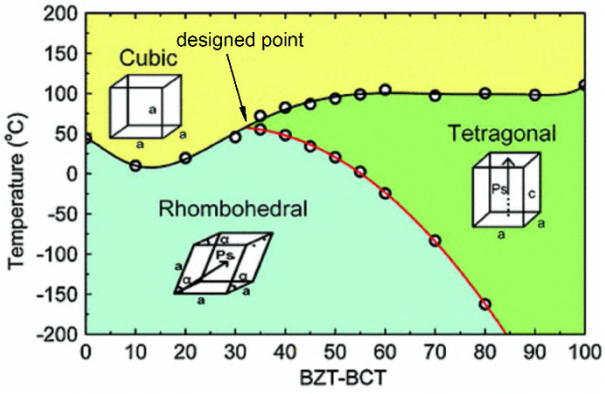
designed point
Cubic
Tetragonal
Rhombohedral
Temperature (°C)
BZT-BCT
200
150
100
50
0
-50
-100
-150
-200
0
10
20
30
40
50
60
70
80
90
100

Figure S1

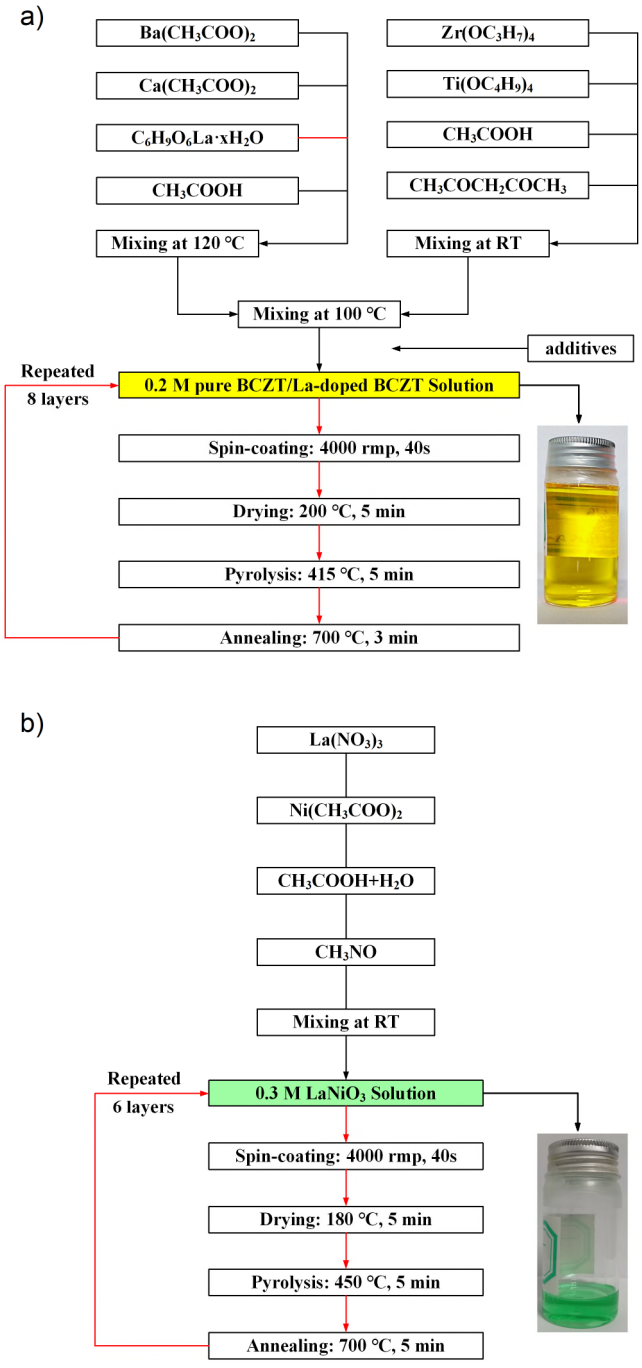
a)
Ba(CH3COO)2
Ca(CH3COO)2
C6H9O6La·xH2O
CH3COOH
Mixing at 120 °C
Zr(OC3H7)4
Ti(OC4H9)4
CH3COOH
CH3COCH2COCH3
Mixing at RT
Mixing at 100 °C
additives
Repeated
8 layers
0.2 M pure BCZT/La-doped BCZT Solution
Spin-coating: 4000 rmp, 40s
Drying: 200 °C, 5 min
Pyrolysis: 415 °C, 5 min
Annealing: 700 °C, 3 min
b)
La(NO3)3
Ni(CH3COO)2
CH3COOH+H2O
CH3NO
Mixing at RT
Repeated
6 layers
0.3 M LaNiO3 Solution
Spin-coating: 4000 rmp, 40s
Drying: 180 °C, 5 min
Pyrolysis: 450 °C, 5 min
Annealing: 700 °C, 5 min

Figure S2

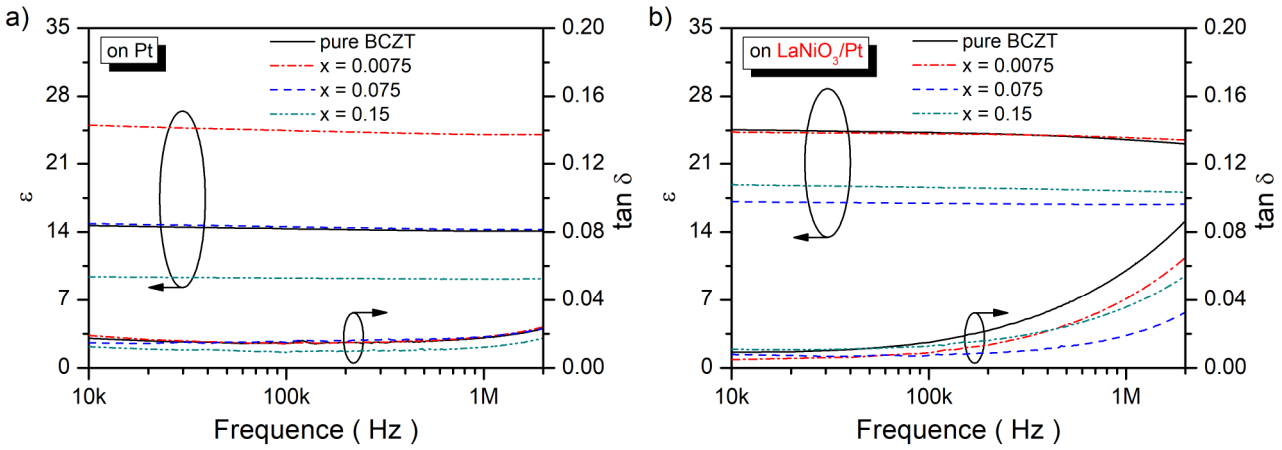
a)
on Pt
pure BCZT
x = 0.0075
x = 0.075
x = 0.15
ε
tan δ
Frequence (Hz)
b)
on LaNiO3/Pt
pure BCZT
x = 0.0075
x = 0.075
x = 0.15
ε
tan δ
Frequence (Hz)

Figure S3

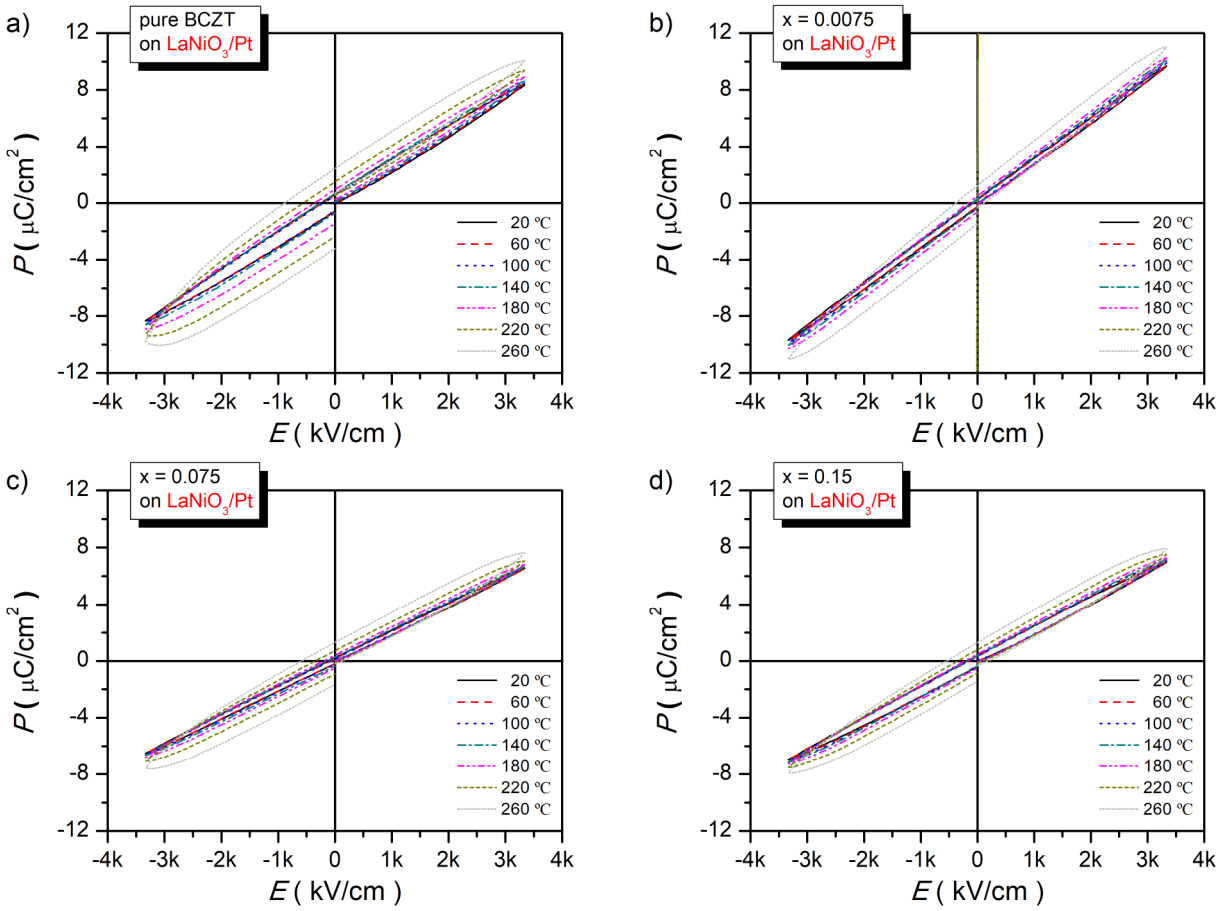
a)
pure BCZT
on LaNiO3/Pt
b)
x = 0.0075
on LaNiO3/Pt
c)
x = 0.075
on LaNiO3/Pt
d)
x = 0.15
on LaNiO3/Pt
P (μC/cm2)
E (kV/cm)
20 ℃
60 ℃
100 ℃
140 ℃
180 ℃
220 ℃
260 ℃

Figure S4

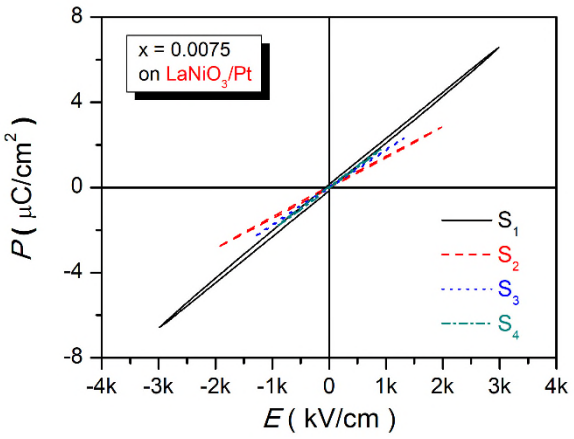
x = 0.0075
on LaNiO3/Pt
S1
S2
S3
S4
P (μC/cm2)
E (kV/cm)
8
4
0
-4
-8
-4k
-3k
-2k
-1k
0
1k
2k
3k
4k

Figure S5

Table S1

Specimens	**S_1**	**S_2**	**S_3**	**S_4**
Area (mm^2)	~ 0.025	~ 0.785	~ 1.802	~ 7.079
W (J/cm^3)	9.5	2.7	1.4	0.7
η (%)	94.6	96.0	94.9	91.4

2019-03-13

High-performance La-doped BCZT thin film capacitors on LaNiO3/Pt composite bottom electrodes with ultra-high efficiency and high thermal stability

He, Shangkai

Elsevier

He S, Peng B, Leighton GJT, et al., (2019) High-performance La-doped BCZT thin film capacitors on LaNiO3/Pt composite bottom electrodes with ultra-high efficiency and high thermal stability. Ceramics International, Volume 45, Issue 9, June 2019, pp. 11749-11755
https://doi.org/10.1016/j.ceramint.2019.03.051